Anharmonic effects in the low-frequency vibrational modes of aspirin and paracetamol crystals

Nathaniel Raimbault,[1,*] Vishikh Athavale,[2] and Mariana Rossi[1,†]

[1]*Fritz-Haber-Institut der Max-Planck-Gesellschaft, Faradayweg 4-6, D-14195 Berlin, Germany*
[2]*Department of Chemistry, University of Pennsylvania, Philadelphia, Pennsylvania 19104, USA*

The low-frequency range of vibrational spectra is sensitive to collective vibrations of the lattice. In molecular crystals, it can be decisive in identifying the structure of different polymorphs and, in addition, it plays an important role in the magnitude of the temperature-dependent component of vibrational free-energy differences between these crystals. We study the vibrational Raman spectra and vibrational density of states of different polymorphs of the flexible aspirin and paracetamol crystals based on dispersion-corrected density functional theory, density functional perturbation theory, and *ab initio* molecular dynamics. We examine the effect of quasiharmonic lattice expansion and compare the results of harmonic theory and the time-correlation formalism for vibrational spectra. Lattice expansion strongly affects the collective vibrations below 300 cm^{-1}, but it is significantly less important at higher frequencies, while thermal nuclear motion can be important in the full vibrational range. We also observe that the inclusion or neglect of many-body van der Waals dispersion interactions does not cause large differences in the low-frequency range of Raman spectra or vibrational density of states, provided the lattice constants are fixed. We obtain quantitative agreement with experimental room-temperature Raman spectra below 300 cm^{-1} for all polymorphs studied. Examining the two-dimensional correlations between different vibrations, we find which modes show a larger degree of anharmonic coupling to others, providing a possible route to assess the accuracy of harmonic free-energy evaluations in different cases.

I. INTRODUCTION

Molecular crystals are a large class of crystals that encompasses common painkillers and antipyretics such as aspirin, paracetamol, or ibuprofen. As suggested by their name, such crystals are built from individual molecular units, which are mainly held together by noncovalent interactions such as hydrogen bonds and dispersion forces. The molecular units that constitute them can be arranged in different patterns and each specific arrangement is called a polymorph. Despite the often small energy differences separating these polymorphs [1], they can present very different physicochemical properties. For instance, paracetamol form II is known to be more soluble than form I, and is also more easily compressible into tablets [2]. Being able to accurately grasp the energetic balance between different polymorphs and to unambiguously characterize them could potentially lead to reduced costs in the pharmaceutical industry, for example. Doing so is no easy task, though: the energy differences between different polymorphs are typically of the order of only a few meV per molecular unit [1] and vibrational structural fingerprints can show only small (but important) differences. Therefore, several factors that compete between each other, such as anharmonic effects in lattice expansion, nuclear vibrations, dispersion forces, and polarization of hydrogen bonds, need to be taken into account [3–5].

Given the large unit cells (containing hundreds of atoms) of some of these molecular crystals, few studies have treated all of these effects in first-principles theoretical calculations [1,3,4,6–8]. Specifically, the impact of anharmonic terms of the potential-energy surface (PES) on the temperature-dependent properties of these crystals has only recently started to be addressed [4,9–14]. In particular, the low-frequency phonon modes, mainly governed by intermolecular interactions (e.g., hydrogen bonds), are sensitive to (anisotropic) lattice expansion at finite temperatures [3,11,15] and also to nuclear fluctuations—even if the extent of this sensitivity has not yet been carefully quantified. This region is particularly important since it strongly contributes to the vibrational free energy at finite temperatures [16]. As an illustration, we show in Fig. 1 the error in the temperature-dependent part of the harmonic vibrational free energy given by a 5% error in the vibrational density of states at different frequencies. Errors in the lower frequencies, especially below 500 cm^{-1}, have a large impact on this term, which becomes more pronounced as the temperature increases.

As vibrational spectra can be measured with high accuracy and at different temperatures, comparing theoretical and experimental spectra in the low-frequency region is important to gauge whether temperature-dependent vibrational free energies can be accurately described by any given theoretical methodology.

In this paper, we present a theoretical characterization of the low-frequency ($\omega < 300$ cm^{-1}) vibrational Raman spectra of the two main polymorphs of paracetamol and aspirin. Comparing these particular polymorphs is enlightening since while for paracetamol the hydrogen-bonding pattern in the

---

*Corresponding author: nathanielraimbault@gmail.com
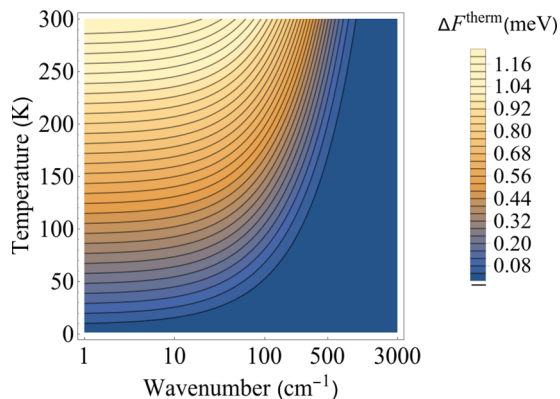†Corresponding author: rossi@fhi-berlin.mpg.de

FIG. 1. Errors in the temperature-dependent term of the harmonic quantum vibrational free energy as a function of temperature T and frequency ω, caused by a percentage error $\Delta\omega$. $\Delta F^{\text{therm}}(\omega, T) = k_B T \ln\left[(1 - e^{-\frac{\hbar(\omega+\Delta\omega)}{k_B T}})/(1 - e^{-\frac{\hbar\omega}{k_B T}})\right]$. We considered $\Delta\omega = 0.05\omega$.

different polymorphs is quite diverse, in aspirin they are almost identical, as shown in Fig. 2(a). We employ density functional theory (DFT) and density functional perturbation theory [17–20] (DFPT), including many-body van der Waals corrections [21,22] (MBD). We present an analysis of how low-frequency vibrational modes change with anharmonic couplings to other modes, with changes in the lattice and with changes in the potential-energy surface.

II. METHODS

In the following, we provide details about the different methodologies we use, as well as the numerical settings we employ in each case. All of our calculations were performed within FHI-aims [23], an all-electron numeric atom-centered-orbitals code. We obtained the experimental crystal structures

from Ref. [24] for aspirin I, from Ref. [25] for aspirin II, and from Refs. [26,27] for paracetamol I and II. We compute energies and forces with the Perdew-Burke-Ernzerhof (PBE) exchange-correlation functional throughout, including MBD dispersion corrections as described in Ref. [28], except where stated otherwise. For the Raman spectra, we calculate the polarizability tensors with DFPT [20]. We calculate the tensors with the local density approximation (LDA) functional, given that we have previously shown in Ref. [20] that it saves considerable computational time and the Raman spectra show no differences when calculating these tensors with different functionals. In the following, it will thus always be assumed that LDA was used for calculating polarizabilities, even if not explicitly mentioned. Unless stated otherwise, a $2 \times 2 \times 2$ k-point grid was used for all polymorphs.

A. Lattice expansion

In order to assess anisotropy in the quasiharmonic lattice expansion calculations, we assumed fixed angles for each molecular crystal polymorph and minimized the second-order Taylor expansion of the Helmholtz free energy F at a particular temperature T,

$$F(a, b, c) = F_0 + \mathbf{p}^t \mathbf{H} \mathbf{p}, \tag{1}$$

where F_0 is the free energy at the equilibrium lattice parameters at the temperature of choice, $\mathbf{H}$ is the matrix of second derivatives of the free energy with respect to the lattice parameters, $\mathbf{p} = (a - a_0, b - b_0, c - c_0)$ where a_0, b_0, and c_0 are the equilibrium unit-cell parameters at a given temperature, and $\mathbf{p}^t$ is its transpose. Given the symmetric nature of $\mathbf{H}$, we thus have 10 unknown variables to determine at a specific temperature T, namely, the six $\mathbf{H}$ matrix elements, the three equilibrium lattice parameters, and F_0. This minimization was done at the assumption of fixed cell angles and employing a nonlinear least-squares fit. We used at least 10 evaluations
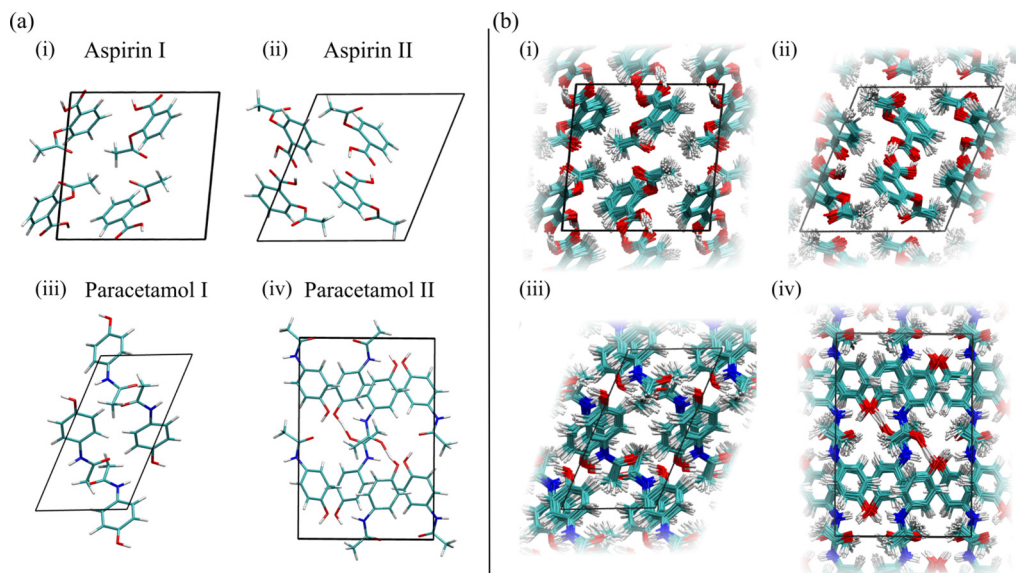

FIG. 2. (a) The four polymorphs of this study at equilibrium: (i) aspirin form I, (ii) aspirin form II, (iii) paracetamol form I, and (iv) paracetamol form II. The unit cell is drawn in black. (b) Superposition of multiple frames coming from an AIMD simulation. In all systems, methyl groups rotate freely. In aspirin form II, the distance between neighboring acetyl groups varies over time.

of F calculated at different values of a, b, and c in the harmonic approximation from DFT (at any given temperature) in order to determine these parameters. Once DFT phonons are obtained for different lattice displacements, the temperature dependence of the vibrational free energy in the harmonic approximation is analytically known, thus making it easy to find the optimum parameters of Eq. (1) at any temperature. Further details of this procedure can be found in the Supplemental Material (SM) [29]. We note that a possible alternative, which would require a comparable amount of phonon evaluations, would be to evaluate mode-specific Grüneisen parameters [30] to approximate the variation of phonon frequency with each lattice parameter.

The *tight* basis sets of FHI-aims were used for all atomic species and the phonon calculations using a $1 \times 1 \times 1$ supercell and a $5 \times 5 \times 5$ q-point grid were performed using the PHONOPY program [31]. We calculated 14 distortions of the lattice for aspirin I, 10 for aspirin II, 15 for paracetamol I, and 13 for paracetamol II. We checked that the solution is a minimum of the free-energy surface by ensuring that the eigenvalues of **H** are all positive. Whenever that was not the case, we displaced the cell in the direction of the eigenvector with the negative eigenvalue, calculated phonons for this displacement, and added this point to the minimization procedure. The routine written for this model is available online [32].

B. Harmonic Raman spectra

A standard way to evaluate vibrational Raman spectra is through the harmonic approximation, in which the Taylor expansion of the potential energy is truncated at the second order. In this procedure, Raman intensities are proportional to the derivatives of the polarizability tensor with respect to atomic displacements (see, e.g., Refs. [33,34]). We calculate the orientation-averaged "powder" harmonic Raman intensity $I_H(\omega)$ (which is directly proportional to the Raman scattering cross section [35]) of a given normal mode p by [36],

$$I_H(\omega) = I_H^\perp + I_H^\parallel \propto \frac{1}{\omega(1 - e^{-\beta\hbar\omega})} \frac{1}{30}\big(10G_p^{(0)} + 7G_p^{(2)}\big),$$

$$G_p^{(0)} = \frac{1}{3}[(\alpha'_{xx})_p + (\alpha'_{yy})_p + (\alpha'_{zz})_p]^2,$$

$$\begin{aligned}G_p^{(2)} = &\frac{1}{2}\big[(2\alpha'_{xy})_p^2 + (2\alpha'_{xz})_p^2 + (2\alpha'_{yz})_p^2\big] \\ &+ \frac{1}{3}\{[(\alpha'_{xx})_p - (\alpha'_{yy})_p]^2 \\ &+ [(\alpha'_{xx})_p - (\alpha'_{zz})_p]^2 + [(\alpha'_{yy})_p - (\alpha'_{zz})_p]^2\},\end{aligned} \quad (2)$$

where $I^\perp$ and $I^\parallel$ are the depolarized and polarized Raman intensities, respectively, $\beta = 1/(k_B T)$, and $(\alpha'_{ij})_p = (\partial\alpha_{ij}/\partial Q_p)_0$ is the derivative of the ij component of the polarizability with respect to the displacement of normal mode Q_p. We compute these derivatives through finite differences, in which we evaluate the polarizability tensor from DFPT [20] at $6N$ (forward and backward) nuclear displacements in the unit cell around the equilibrium position, with N being the number of atoms per unit cell. We use regular Cartesian coordinates to describe normal modes. This coordinate system may not always be appropriate when dealing with torsional vibrational modes, for which a better approach is to use curvilinear

coordinates [37]. Knowing the space group of our crystals, we then apply all symmetry operations pertaining to this group onto the vibrational modes, in order to confirm whether or not they should show Raman activity [38]. *A posteriori*, we discard modes that are Raman inactive, if any are found. We note, however, that selection rules are naturally enforced by the whole procedure and such an *a posteriori* correction is only needed if (rare) numerical errors are present.

The harmonic Raman spectra presented in this paper were calculated with *light* numerical and basis-set settings in the FHI-aims code [23], for direct comparison with the anharmonic spectra. Differences between *light* and *tight* harmonic spectra are minor and shown in Fig. S3 in the SM [29].

C. Anharmonic Raman spectra

A way to go beyond the harmonic approximation is to resort to the time-correlation formalism. In this formalism, the potential energy is sampled without any approximations, thus ensuring that full anharmonicity (here at a classical nuclei approximation) is captured. Vibrational Raman line shapes are proportional to the Fourier transform of the static electronic polarizability (or static electronic susceptibility) autocorrelation function [39]. Realizing this formalism requires computing polarizability tensors along molecular dynamics trajectories, as explained in, e.g., Ref. [20]. For comparison with experimental spectra taken from powder samples, here we calculate the anharmonic powder-averaged Raman intensity $I_A(\omega)$. This can be calculated from the isotropic and anisotropic contributions to the signal as follows (see Ref. [40], Eqs. (21)–(99) and (21)–(100); and also [35]):

$$I_A(\omega) = I_A^\perp + I_A^\parallel = I_{\text{iso}}(\omega) + \frac{7}{3}I_{\text{aniso}}(\omega),$$

$$I_{\text{iso}}(\omega) = I_A^\parallel - \frac{4}{3}I_A^\perp \propto \int_{-\infty}^{+\infty} dt\, e^{-i\omega t}\langle\bar{\alpha}(0)\bar{\alpha}(t)\rangle,$$

$$I_{\text{aniso}}(\omega) = I_A^\perp \propto \int_{-\infty}^{+\infty} dt\, e^{-i\omega t}\frac{1}{10}\langle\text{Tr}[\boldsymbol{\beta}(0)\cdot\boldsymbol{\beta}(t)]\rangle, \quad (3)$$

where the electronic polarizability (or electronic susceptibility) tensor $\boldsymbol{\alpha} = \bar{\alpha}\mathbf{I} + \boldsymbol{\beta}$ and the brackets $\langle\cdot\rangle$ denote the canonical average. Here we consider only the electronic contribution to the dielectric permittivity. In ionic and polar crystals, contributions from ionic polarization could be more pronounced, as discussed in Ref. [41]. We apply the so-called quantum or Kubo-transform correction factor to the line shapes of $\beta\hbar\omega/(1 - e^{-\beta\hbar\omega})$.

All of our *ab initio* molecular dynamics (AIMD) simulations were performed with *light* numerical and basis-set settings in FHI-aims and otherwise the same settings as for all other calculations. We performed a thermalization (NVT) run of about 2 picoseconds for each polymorph, followed by two NVE simulations of 15 picoseconds each, using a time step of 0.5 femtosecond. We computed polarizability tensors with DFPT calculations every 1 fs.

D. 2D-correlation spectra

Two-dimensional (2D) correlation spectra can be calculated from our MD simulations. We follow the procedure

detailed in Ref. [42]. These 2D correlations "provide a quantitative comparison of spectral density variations observed at two different spectral variables over some finite observation interval T_{min} and T_{max}" [42]. It is thus a useful tool to understand couplings between different modes, as has been recently shown for the case of water [43]. We recall the main formulas from Ref. [42] to produce such spectra in the present text. We define the dynamic spectrum $\tilde{I}_j(\omega)$ as

$$\tilde{I}_j(\omega) = I_j(\omega) - \bar{I}(\omega), \tag{4}$$

where $I_j(\omega)$ is simply the intensity [e.g., Raman intensity as defined in Eq. (3)] at ω, evaluated for a given time window T_{win}, the duration of which depends on the phenomenon one wants to observe. If we divide our trajectory of interval $[T_{min}, T_{max}]$ into m segments of length T_{win} evenly spaced by an increment of $(T_{max} - T_{min})/(m - 1)$, the average spectrum $\bar{I}(\omega)$ is given by

$$\bar{I}(\omega) = \frac{1}{m} \sum_{j=1}^{m} I_j(\omega), \tag{5}$$

and the synchronous 2D correlation intensity takes the following expression:

$$\phi(\omega_1, \omega_2) = \frac{1}{m-1} \sum_{j=1}^{m} \tilde{I}_j(\omega_1)\tilde{I}_j(\omega_2). \tag{6}$$

In all of our simulations, we choose $T_{win} = 1$ ps.

The diagonal peaks appearing in these spectra are referred to as autopeaks and are always positive; they represent the change in intensity at a given frequency over a given period of time. Hence, regions that vary substantially in intensity will have strong autopeaks, while regions that vary little will have weak autopeaks. Off-diagonal peaks, or cross peaks, correspond to simultaneous changes (of equal or opposite signs) in intensities at two different frequencies over a given duration, indicating a probable coupling between the two corresponding vibrational modes.

III. RESULTS

A. Lattice expansion and harmonic Raman spectra

The four molecular crystals studied in this work, namely, aspirin I and II, and paracetamol I and II, have known crystal

structures, which are shown in Fig. 2(a). In many molecular-crystal polymorphs, important structural differences can already be spotted simply by looking at the molecular arrangement and the shape of the unit cell, even without resorting to Raman spectroscopy. Paracetamol I and II are good examples of such different polymorphs, as shown in Fig. 2(a). For a few, however, differences are much more subtle. This is particularly true for aspirin, for which both forms appear to have the same structure in projection. One key difference lies in the pattern formed by intermolecular hydrogen bondings between the acetyl groups (CH_3CO) [44–48].

Lattice expansion can have a large impact on the energetics, affecting the stability ranking of polymorphs [49]. However, here we will focus on its impact on vibrational spectra and, more specifically, on Raman spectra. To this end, we calculate the harmonic Raman spectra (see Sec. II B) of aspirin I and II, using for each of them two different lattice parameters: the experimentally determined ones obtained from Refs. [24,26,27,44] and the ones coming from the procedure outlined in Sec. II A. The lattice parameters we use are given in Table I.

We observe that most calculated lattice parameters at 300 K are relatively close to the experimental 300 K results, although the changes are quite heterogeneous. The most notable differences can be seen for the b parameter of paracetamol II and the c parameter of aspirin II that both show a difference of about 2.8%. The absolute values of the calculated lattice constants at 300 K for form I of paracetamol and aspirin are closer to experiment than those of their respective form II, although the relative expansion is better reproduced for the latter (see SM, Fig. S1 [29]). Other works have been conducted on a similar topic, but employing different functionals and a different approach, as they fixed the experimentally determined volumes at different temperatures and only optimized the lattice parameters, leading to an expected good agreement with experimental values [50]. We draw attention to the fact that lattice parameters calculated without van der Waals (VdW) dispersion interactions (at the potential-energy surface), shown in Table I, strongly deviate from experimental values, highlighting the importance of these interactions in determining the shape and density of these crystals.

The harmonic Raman spectra of aspirin form I and II computed with our calculated lattice parameters and the experimental ones at 300 K are shown in Fig. 3. We observe that

TABLE I. Lattice parameters. Unit vectors are in Å and angles in degrees. Second and third columns: fully (atomic positions and unit cell) optimized structure at the potential-energy surface (PES) using the PBE and the PBE+MBD functional. Fourth column: calculated lattice constants from our quasiharmonic lattice expansion scheme, calculated with the PBE+MBD functional. Fifth column: experimental lattice constants at 300 K from Refs. [24,26,27,44]. Last column: error (in percentage) between the calculated and experimental lattice parameters at 300 K.

|	PES (PBE)				PES (PBE+MBD)				Calc. 300 K				Expt. 300 K				Δ (Calc.-Expt.) (%)		
	a	b	c	β	a	b	c	β	a	b	c	β	a	b	c	β	Δa	Δb	Δc
Paracetamol I	6.92	12.51	12.98	55.8	7.01	9.15	12.77	66	7.09	9.23	12.75	66	7.08	9.34	12.85	64.5	0.14	1.18	0.78
Paracetamol II	11.63	9.14	17.40	90	11.59	7.30	17.26	90	11.62	7.61	17.26	90	11.83	7.40	17.16	90	1.78	2.84	0.58
Aspirin I	12.30	7.00	12.30	96	11.40	6.52	11.33	96	11.50	6.51	11.46	96	11.42	6.60	11.48	96	0.70	1.36	0.17
Aspirin II	13.26	6.85	12.38	114	12.27	6.43	11.35	111	12.52	6.65	11.82	111	12.36	6.53	11.50	112	1.29	1.84	2.78
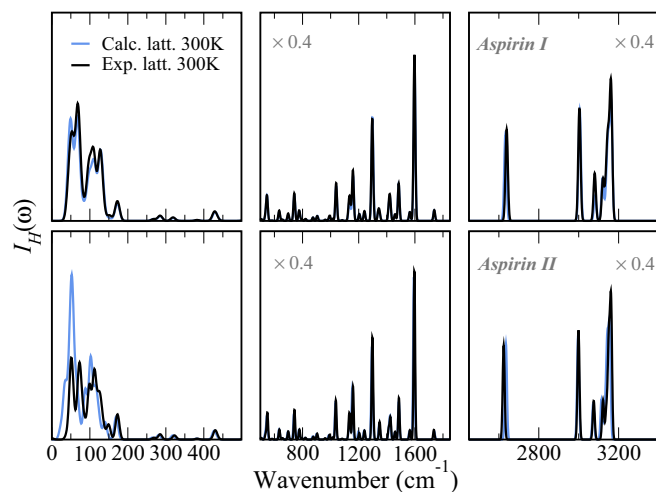
FIG. 3. Harmonic Raman spectra of aspirin I (top) and II (bottom) obtained with the experimental lattice parameters (black lines) and the calculated lattice parameters (blue lines) at 300 K. We used the PBE+MBD functional. In the middle and right panels, we indicate the factor by which each panel is scaled as compared to the left panel.
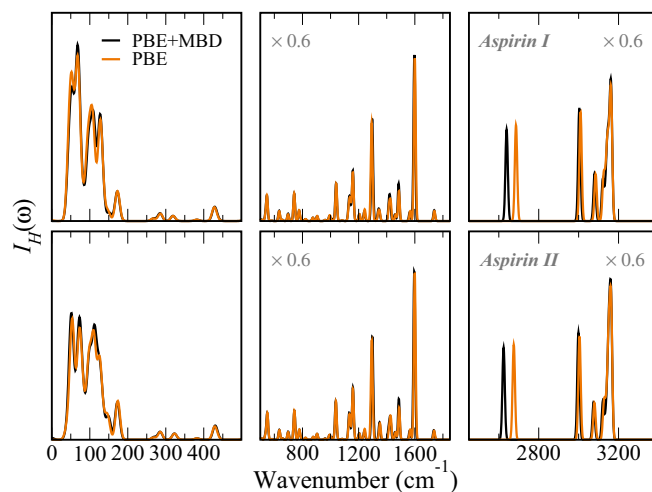

FIG. 4. Harmonic Raman spectra of aspirin I (top) and II (bottom) obtained with the PBE (orange) and the PBE+MBD (black) functionals, using the 300 K experimental lattice constants.

using different lattice parameters has seemingly no influence in the middle-frequency range, while at high frequencies, only small rigid shifts and minor changes in intensities can be observed. The impact is most easily seen at low frequency, especially for form II, where the intensities of several peaks are modified and the general line shape changes substantially.

It is not surprising to see that the changes manifest mostly at low frequency since, as mentioned in Sec. I, low-frequency phonon modes tend to be sensitive to the intermolecular potential, which is determined by the shape of the lattice. The differences between the two polymorphs can stem from different factors. As we have previously seen, the difference between the experimental lattice constants and the calculated ones is greater for aspirin II than aspirin I, so it is only logical that this difference is reflected in the spectrum. Also, it is known that aspirin II is more easily compressible, as it forms flat hydrogen-bonded sheets along the c axis, as opposed to a wavelike pattern in form I [46]. This seems to be consistent with the larger expansion of the c lattice vector of aspirin II, which is observed both in our calculations and in experiments, even though the differences between both polymorphs are rather small. In any case, it is very interesting to notice that relatively moderate changes in lattice parameters can translate to a more noticeable change on the low-frequency range of the harmonic Raman spectrum.

The lattice is not the only parameter that may impact a vibrational spectrum. Another worthwhile aspect to consider is the exchange-correlation functional that is used, or the addition of van der Waals dispersion. Especially for systems such as molecular crystals, dispersion forces are known to play an important role and change the energetics substantially [5]. We report the impact of dispersion interaction on the harmonic Raman spectra of the same aspirin polymorphs in Fig. 4. In order to decouple different effects, we maintain the experimental lattice parameters in this case, but fully optimize the atomic positions with the different potential-energy surfaces.

We observe that at high frequencies, ignoring van der Waals contributions in this case results in a blueshift of 47 (51) cm^{-1} of the peak located at 2639 (2624) cm^{-1} for aspirin I (II). This peak corresponds to symmetric O-H stretching motions between the molecular dimers. We note that we observe a similar shift of this band when simulating these spectra using 300 and 123 K experimental lattice parameters (see SM, Fig. S2 [29]). These observations are consistent with the fact that removing van der Waals interactions from the model weakens the H bonds, and so does increasing the temperature. Consequently, these two effects lead to a blueshift of this band. The middle- and low-frequency ranges remain basically unaltered by the change of functional. We note that in the geometries considered here, we observe the presence of a vibrational mode at 33 cm^{-1} in both polymorphs when including MBD corrections. The same modes are at 34 cm^{-1} when neglecting MBD corrections. These are not Raman-active modes, though, and hence do not show up in Fig. 4.

The results presented so far confirm the importance of taking lattice expansion into account when assessing Raman spectra. The discrepancies we observe in our calculated lattice constants at 300 K, in comparison to experiment, can be due to several factors, among them the exchange-correlation functional and the approximations in the lattice-expansion procedure itself [for instance, the assumption of fixed angles or the fact that the multiparameter optimization of Eq. (1) can lead to metastable minima]. A detailed investigation of this issue requires studying a broader set of crystals, functionals, and a careful benchmark between different methods (including carrying out computationally costly constant-pressure AIMD simulations at different temperatures directly). This will be the subject of a future study. For the remainder of the present work and in order to focus solely on the impact of vibrational anharmonic contributions, we maintain the experimental lattice parameters (see Table I) for aspirin I, II, paracetamol I, and the one reported in Ref. [51] for paracetamol II.
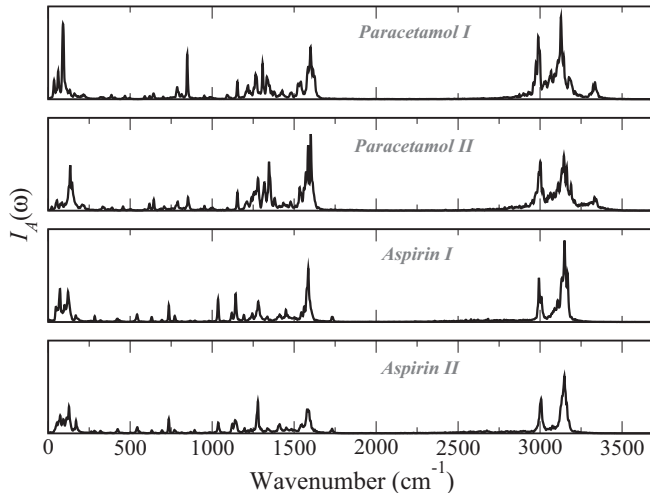
FIG. 5. Anharmonic Raman spectra of the four polymorphs of this study on the whole frequency range calculated from AIMD at 300 K with the PBE+MBD functional. Here the intensities have been scaled by a frequency-dependent factor of $\sqrt{\omega}$ solely for visualization purposes, i.e., so that high frequencies become as visible as low frequencies.

B. Anharmonic effects on vibrational modes and Raman line shapes

Figure 2(b) shows the pronounced nuclear fluctuations that are observed at room temperature. We note, for example, that during AIMD simulations, in all cases the methyl (CH$_3$) groups rotate freely and we observe hydrogen-transfer events between two aspirin monomers. Other torsional motions within the molecular units are also activated, for example the rotation of the aromatic ring with respect to the rest of the molecules. The question is how these fluctuations translate to the vibrational Raman spectra.

The time-correlation formalism gives access to the full anharmonicity of the potential-energy surface within the approximation used for the dynamics of the nuclei (e.g., classical or quantum). It is thus able to capture combination bands, overtones, and the phonon lifetimes that give rise to the anharmonic line shape. A drawback of this formalism is that the assignment of vibrational modes is not straightforward and it is often based on the corresponding harmonic spectrum, for which modes are well defined [52]. Techniques have been proposed to extract effective vibrational modes directly from AIMD simulations [53,54]. Such techniques, although very successful in small molecules, require large sampling times and are not straightforward to apply to larger and very flexible systems or to simulations that incorporate nuclear quantum statistics.

In Fig. 5, we show the calculated anharmonic Raman spectra in the full frequency range [55]. The most interesting observation regarding the high-frequency region is that the intense peak observed at 2639 (2624) cm^{-1} for aspirin I (II) in the harmonic approximation, corresponding to the stretch of O-H bonds that connect the H-bonded aspirin dimers in the crystal, seems to be completely absent from the anharmonic spectra and, in fact, also from experiments,
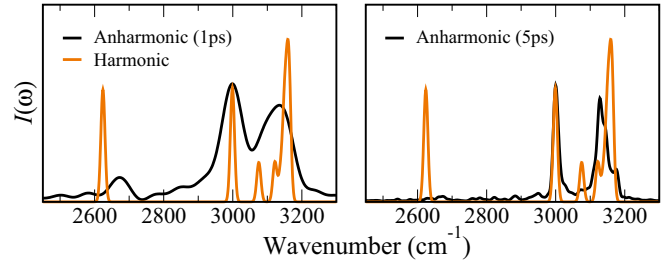

FIG. 6. Evolution of the anharmonic Raman spectrum of aspirin II for different simulation lengths as compared to the harmonic Raman spectrum. In each case, the height of the anharmonic peak located at 3000 cm^{-1} has been adjusted to the harmonic one. Note that the same effect is also observed for aspirin I.

as shown in Ref. [56]. However, when calculating Raman spectra from short-time (1 ps) autocorrelation functions of the polarizability tensors, one can see that this peak is present, but gets broadened and loses intensity upon increasing simulation time, as shown in Fig. 6 [we also show in the SM [29], Fig. S6, that this vibration is actually present in the vibrational density of states (VDOS) of the hydrogen involved in this mode]. In addition, this mode is connected to the observed hydrogen-transfer events between two aspirin monomers, which we expect to become more pronounced or turn into a fully shared hydrogen if nuclear quantum effects are included.

As shown in the SM [29], Fig. S4, and further discussed in the next section, neglecting vdW contributions in the anharmonic Raman spectra of all crystals results in only small changes to the line shapes and intensities, as long as the lattice parameters are kept fixed at the same values.

In Fig. 7, we focus on the structure-sensitive low-frequency range of these spectra. We compare our harmonic and anharmonic spectra to experimental results for aspirin and paracetamol obtained from powder samples at room temperature, as reported in Refs. [45] and [57], respectively. For visual comparison, we normalized to 1 the highest peak of each spectrum. For both systems, there is a good visual agreement between the harmonic Raman spectra and the experimental spectra. There are significant shifts between the harmonic and anharmonic Raman spectra for only a subset of the peaks in this region, which shift closer to the position observed in experiment when anharmonicity is included. For clarity, we label some of these peaks and depict their harmonic normal mode of vibration in Fig. 7, noting that for each system, there are both localized vibrational modes (here typically methyl group rotations) and more global-motion modes. We will see in the next section that the more pronounced shifts of the collective modes correspond to vibrations that have a stronger correlation with other modes. While none of the approaches allows us to reach a perfect quantitative agreement with experiment, the anharmonic spectra provide an overall better description of peak positions, in particular for paracetamol I and II. Some of the discrepancies in relative intensities could be resolved by increasing statistical sampling. We highlighted some of the main frequency shifts between harmonic and anharmonic results by placing a vertical dotted line.
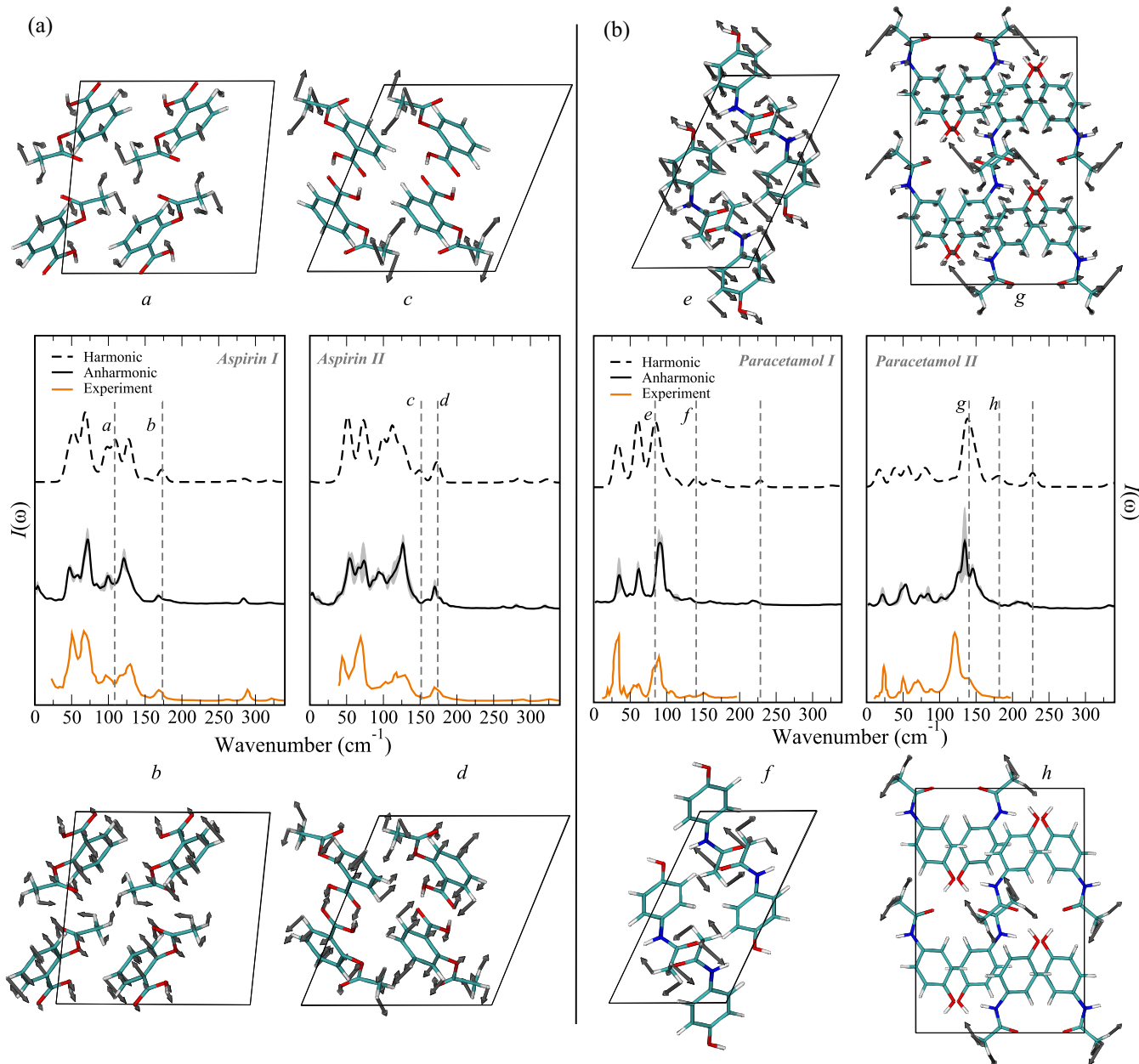
FIG. 7. Comparison of the PBE+MBD harmonic, anharmonic (300 K), and experimental (300 K) Raman spectra of aspirin I and II, and paracetamol I and II. The experimental data were extracted from Refs. [45] and [57]. The shaded areas around the anharmonic spectra indicate the uncertainty derived from the statistical error of the different trajectories. Selected normal modes from the harmonic analysis are also shown, for which the arrows represent the direction and the amplitude of the moving atoms. The unit cell is drawn in black.

C. Mode coupling

In order to further analyze the effects of anharmonic mode coupling in the low-frequency vibrational range of these crystals, we turn our attention to the vibrational density of states (VDOS), which here we also calculate within the time-correlation formalism by summing the Fourier transforms of the atomic velocity autocorrelation functions. This quantity plays a more direct role in the estimation of the vibrational free energies of these crystals. Experimentally, only inelastic neutron scattering can directly access the VDOS and such measurements are rare for most materials.

We report the VDOS of paracetamol I, aspirin I, and aspirin II in Fig. 8 with the PBE and PBE+MBD functionals (data for paracetamol II and the PBE+MBD functional are shown in the SM [29], Fig. S5). We note that in all cases, the VDOS is almost insensitive to the inclusion of many-body dispersion in the whole frequency range, an assertion that also holds for the harmonic VDOS when using the same lattice constants (see SM [29], Fig. S6). It thus appears that anharmonic contributions play a more important role than the inclusion or not of vdW effects, *if* the lattice parameters are kept constant (we stress that vdW are extremely important when it comes to relaxing unit-cell parameters).
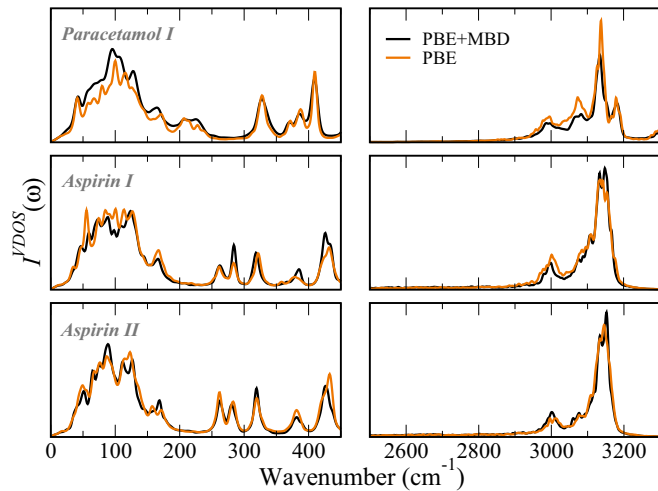
FIG. 8. VDOS spectra of (from top to bottom) paracetamol I, aspirin I, and aspirin II obtained with the PBE (orange line) and PBE+MBD (black line) functionals.

In order to characterize mode coupling, we calculate the 2D VDOS correlation spectra as explained in Sec. II D. Our results are shown in Fig. 9 for all four polymorphs presented in this study. For each 2D-correlation plot, we make two cuts. The first cut corresponds to the lowest observed frequency of the system, while the second one is meant to highlight a difference in intermode couplings between polymorphs. Additionally, we focus on correlations within the $0–900$ cm^{-1} region only. The following assignment of vibrational modes

will be based on results from the harmonic approximation, albeit knowing that frequency shifts may be present. We choose each time the most probable eigenmode, i.e., the one corresponding to the closest harmonic eigenfrequency.

Overall, we observe that most of the vibrational modes showing stronger frequency shifts in Fig. 7 are also the ones showing stronger correlations with other modes in Fig. 9. For example, for aspirin I, the mode around 120 cm^{-1} which marks the edge of the intense low-frequency Raman signal is considerably shifted in the anharmonic case, and it is seen to show a pronounced anticorrelation to the mode located at 49 cm^{-1} (bending motion of one of the radicals of the benzene ring). Another example is the peak labeled e of paracetamol I in Fig. 7. It shows several pronounced anticorrelations around 366 cm^{-1} (bending motion of the benzene ring), 465 cm^{-1} (C-O bendings in the benzene plane and rocking of the benzene), and 630 cm^{-1} (breathing mode of the benzene rings). In the following, we discuss other noteworthy aspects of these 2D correlations, which evidence differences between the sets of polymorphs.

For aspirin I, the lowest observed frequency at around 35 cm^{-1} corresponds to a "sliding motion" of the molecules with respect to one another. It couples in particular to a high-frequency mode at about 740 cm^{-1} that mainly consists of a wagging motion of the benzene ring. The second vibration we focus on, at around 430 cm^{-1}, corresponds to collective motions involving, in the majority, CO and CC bending motions. It couples positively most strongly to two other modes at 155 and 310 cm^{-1}, corresponding, respectively, to methyl group rotations (rocking) and bendings between methyl groups and their radicals.
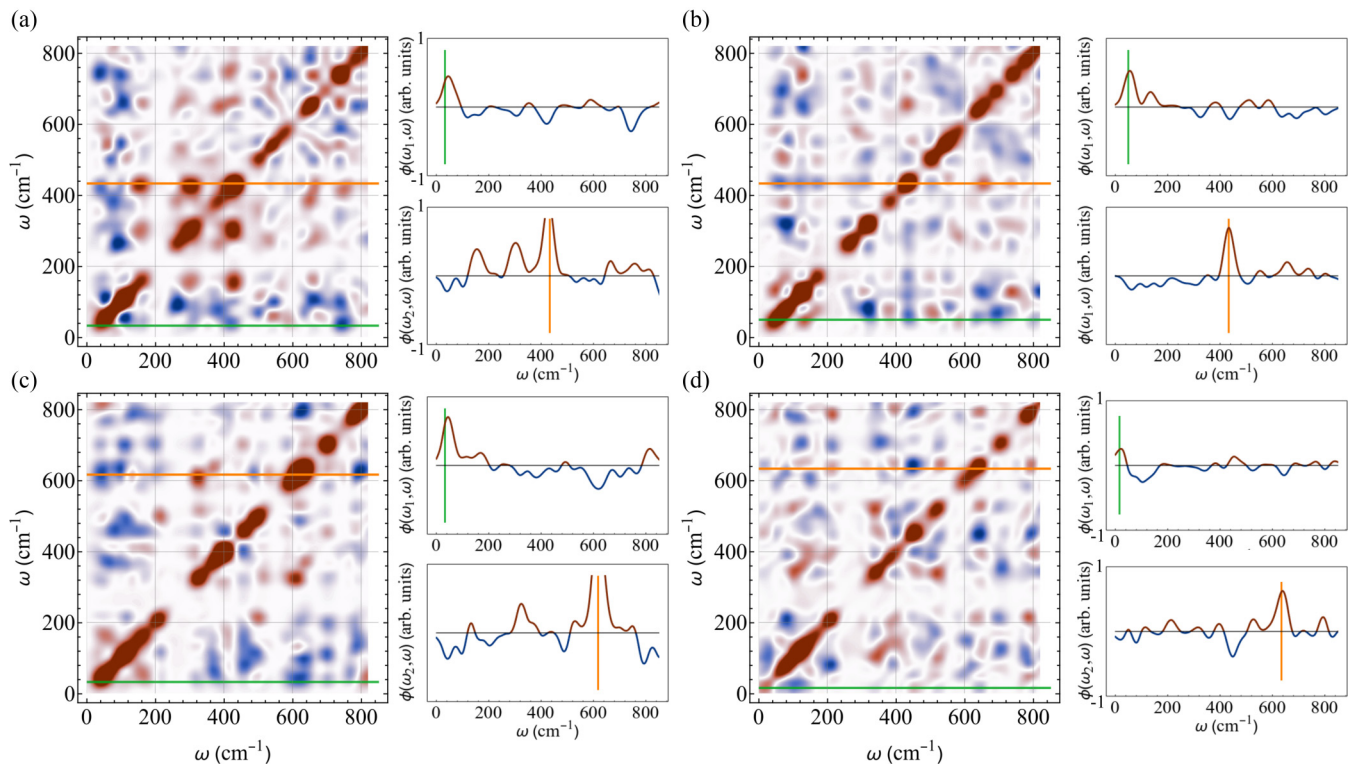

FIG. 9. VDOS 2D correlation spectra of (a) aspirin I, (b) aspirin II, (c) paracetamol I, and (d) paracetamol II. Blue (red) indicates a negative (positive) correlation between modes, i.e., the intensities of a given pair vary in the opposite (same) direction. $T_{\text{win}} = 1$ ps.

For aspirin II, the 35 cm^{-1} mode (analogue to that of aspirin I) couples most strongly (and positively) to the mode at 130 cm^{-1}, which corresponds to collective partial methyl group rotations and bending motions between benzene rings and their radicals. The second cut at 430 cm^{-1} (analogous to that of aspirin I) shows only weak correlation to other modes, in stark contrast to aspirin I.

For paracetamol I, the lowest-frequency vibration around 35 cm^{-1} (involving small rotations of the individual molecular units as a whole) shows a pronounced coupling with another mode at 630 cm^{-1}, consisting, for the most part, of C-C bendings. Similarly, the second mode we pick at 630 cm^{-1} shows, in particular, two couplings at 35 cm^{-1} and 800 cm^{-1}, with the latter consisting of N-H, C-H, and O-H bending motions, without twisting the backbone structure.

For paracetamol II, one observes that in the low-frequency region, the lowest-energy mode at about 16 cm^{-1} (sliding motion of the molecules with respect to one another) couples very little to higher-frequency vibrations. Conversely, the intense mode at 630 cm^{-1}, which is extremely similar to that of paracetamol I, has a strong negative coupling with a mode at 450 cm^{-1}, composed mainly of C-O and C-N bendings.

All the vibrational modes mentioned above can be visualized in the SM [29], Figs. S10–S13. In general, there is no unique coupling between two specific vibrational modes, but rather a complex pattern of correlations between several of them in this low-frequency range composed of delocalized modes. This serves as a guide to understand which polymorphs and in which frequency regions one can expect more changes due to anharmonic effects and can thus serve as a diagnostic tool as to whether harmonic evaluations of free energy will be more or less accurate. We plan to further explore this aspect in the future.

IV. CONCLUSIONS

In this paper, we calculated harmonic and anharmonic Raman spectra of two polymorphs of paracetamol and aspirin, using a recent implementation of DFPT in the FHI-aims code and focusing especially in the low-frequency range, below 300 cm^{-1}. We studied the impact of quasiharmonic lattice expansion over harmonic Raman spectra, and concluded that while the middle- and high-frequency ranges are almost insensitive to moderate changes in lattice parameters, the low-frequency harmonic Raman spectra show important changes. We also measured the influence of many-body dispersion corrections, both in harmonic and anharmonic Raman spectra and vibrational density of states at fixed experimental lattice parameters. In the harmonic picture, the impact of MBD for both Raman and VDOS spectra is almost negligible. In the anharmonic picture at room temperature, the impact of adding MBD interactions is overall very tenuous. Dispersion interactions are, nevertheless, extremely important for determining the lattice parameters and the thermal lattice expansion in these crystals, as one would expect given the nature of the intermolecular interactions. We compared anharmonic Raman spectra below 300 cm^{-1} to experimental room-temperature spectra of all polymorphs, obtaining good agreement. Finally, we reported VDOS 2D-correlation spectra and showed that different correlations exist between low- and higher-frequency

vibrational modes, suggesting a high degree of anharmonicity for specific modes, but not for others. Interestingly, similar vibrational modes in different polymorphs show very different correlation patterns to other modes.

Overall, our results show that vibrational properties calculated from AIMD can accurately describe the low-frequency as well as the high-frequency vibrational region of molecular crystals and reproduce the finer line-shape structure, provided that enough statistical sampling is performed. The harmonic approximation does reproduce the main experimental peaks as well, even though several peaks are shifted with respect to anharmonic results, especially for paracetamol. We observe that the most pronounced peak shifts in the low-frequency range correlate with stronger off-diagonal correlation in our 2D-correlation spectra. This means that temperature-dependent free-energy calculations based on AIMD [4] can indeed serve as benchmark values for such crystals, provided the cost of such simulations is affordable and a good estimation of the lattice constants at different temperatures is possible, either through simulations or experiment.

The results also highlight once more the complexity of studying systems such as molecular crystals, the structure and properties of which depend on a delicate interplay between several phenomena. Cheaper methods such as the harmonic approximation give very valuable insights into these structures, but are by essence bound to fail for anharmonic modes and high temperatures. In the present study, the most dramatic failure of the harmonic approximation was observed in the high-frequency OH-stretch mode of the aspirin crystals. The calculation of 2D-correlation spectra could allow one, in principle, to assess the validity of harmonic free-energy evaluations, given that weak intermode correlations suggest that anharmonic effects are less important. This aspect could be exploited in the future.

For a more thorough understanding and assessment of polymorphic molecular crystals, the anharmonic route thus seems to be unavoidable if one can overcome the cost of such simulations in large-scale studies. As an example, the calculation of the trajectories needed to obtain the anharmonic Raman spectrum of paracetamol I required about 300 000 core hours (around 75 000 for the dynamics and 225 000 for the computation of polarizabilities) in the COBRA supercomputer (processor type Intel Skylake 6148). This cost breakdown suggests that efficiently modeling the electric-field response properties could represent a larger gain in time than employing a good model to calculate the forces. Machine-learning approaches can be employed in this case, as will be demonstrated in an upcoming paper [58]. Such a reduction in computational cost will allow the study of a much wider range of systems, including also nuclear quantum effects.

The data presented in this work as well as the input and output files used to produce it are publicly available as a dataset [59] in the NOMAD Repository.

[1] A. M. Reilly *et al.*, Acta Crystallogr. Sect. B **72**, 439 (2016).

[2] L. H. Thomas, C. Wales, L. Zhao, and C. C. Wilson, Cryst. Growth Des. **11**, 1450 (2011).

[3] J. Hoja, A. M. Reilly, and A. Tkatchenko, Wiley Interdiscip. Rev. Comput. Mol. Sci. **7**, e1294 (2016).

[4] M. Rossi, P. Gasparotto, and M. Ceriotti, Phys. Rev. Lett. **117**, 115702 (2016).

[5] J. Hoja and A. Tkatchenko, Faraday Discuss. **211**, 253 (2018).

[6] G. M. Day, Crystallogr. Rev. **17**, 3 (2011).

[7] S. S. L. Price, Acc. Chem. Res **42**, 117 (2009).

[8] S. L. Price and S. M. Reutzel-Edens, Drug Discov. Today **21**, 912 (2016).

[9] A. Ø. Madsen, B. Civalleri, M. Ferrabone, F. Pascale, and A. Erba, Acta Crystallogr. Sect. A **69**, 309 (2013).

[10] M. Z. Brela, M. J. Wójcik, Ł. J. Witek, M. Boczar, E. Wrona, R. Hashim, and Y. Ozaki, J. Phys. Chem. B **120**, 3854 (2016).

[11] M. T. Ruggiero, J. A. Zeitler, and A. Erba, Chem. Commun. **53**, 3781 (2017).

[12] J. Hoja, H.-Y. Ko, M. A. Neumann, R. Car, R. A. DiStasio, and A. Tkatchenko, Sci. Adv. **5**, eaau3338 (2019).

[13] C. Červinka, M. Fulem, R. P. Stoffel, and R. Dronskowski, J. Phys. Chem. A **120**, 2022 (2016).

[14] J. G. Brandenburg, J. Potticary, H. A. Sparkes, S. L. Price, and S. R. Hall, J. Phys. Chem. Lett. **8**, 4319 (2017).

[15] G. J. O. Beran, J. D. Hartman, and Y. N. Heit, Acc. Chem. Res. **49**, 2501 (2016).

[16] M. Rossi, M. Scheffler, and V. Blum, J. Phys. Chem. B **117**, 5574 (2013).

[17] X. Gonze, Phys. Rev. B **55**, 10337 (1997).

[18] X. Gonze and C. Lee, Phys. Rev. B **55**, 10355 (1997).

[19] J. Gerratt and I. M. Mills, J. Chem. Phys. **49**, 1719 (1968).

[20] H. Shang, N. Raimbault, P. Rinke, M. Scheffler, M. Rossi, and C. Carbogno, New J. Phys **20**, 073040 (2018).

[21] A. Tkatchenko, R. A. DiStasio, R. Car, and M. Scheffler, Phys. Rev. Lett. **108**, 236402 (2012).

[22] A. Ambrosetti, A. M. Reilly, R. A. DiStasio, and A. Tkatchenko, J. Chem. Phys. **140**, 18A508 (2014).

[23] V. Blum, R. Gehrke, F. Hanke, P. Havu, V. Havu, X. Ren, K. Reuter, and M. Scheffler, Comput. Phys. Commun. **180**, 2175 (2009).

[24] C. C. Wilson, New J. Chem. **26**, 1733 (2002).

[25] S. Varughese, M. S. R. N. Kiran, K. A. Solanko, A. D. Bond, U. Ramamurty, and G. R. Desiraju, Chem. Sci. **2**, 2236 (2011).

[26] T. N. Drebushchak and E. V. Boldyreva, Z. Kristallogr. Cryst. Mater. **219**, 506 (2004).

[27] C. C. Wilson, Z. Kristallogr. Cryst. Mater. **215**, 693 (2000).

[28] R. A. Distasio, Jr., V. V. Gobre, and A. Tkatchenko, J. Phys. Condens. Matter **26**, 213202 (2014).

[29] See Supplemental Material at http://link.aps.org/supplemental/10.1103/PhysRevMaterials.3.053605 for additional detail about the present work.

[30] Y. N. Heit and G. J. O. Beran, Acta Crystallogr. Sect. B **72**, 514 (2016).

[31] A. Togo and I. Tanaka, Scr. Mater. **108**, 1 (2015).

[32] V. Athavale, N. Raimbault, and M. Rossi, https://github.com/sabia-group/lattice_expansion.

[33] J. Neugebauer, M. Reiher, C. Kind, and B. A. Hess, J. Comput. Chem. **23**, 895 (2002).

[34] M. Veithen, X. Gonze, and P. Ghosez, Phys. Rev. B **71**, 125107 (2005).

[35] W. F. Murphy, M. H. Brooker, O. F. Nielsen, E. Praestgaard, and J. E. Bertie, J. Raman Spectrosc. **20**, 695 (1989).

[36] S. A. Prosandeev, U. Waghmare, I. Levin, and J. Maslar, Phys. Rev. B **71**, 214307 (2005).

[37] V. V. Rybkin and U. Ekström, J. Chem. Phys. **141**, 064108 (2014).

[38] From group theory, for a mode to be Raman active, it needs to have the same symmetry as a component of the polarizability tensor, i.e., x^2, y^2, z^2, xy, xz, or yz.

[39] S. Mukamel, *Principles of Nonlinear Optical Spectroscopy*, Oxford Series in Optical and Imaging Sciences (Oxford University Press, Oxford, 1995).

[40] D. McQuarrie, *Statistical Mechanics* (University Science Books, Mill Valley, California, 2000).

[41] A. Calzolari and M. B. Nardelli, Sci. Rep. **3**, 2999 (2013).

[42] I. Noda, A. E. Dowrey, C. Marcoli, G. M. Story, and Y. Ozaki, Appl. Spectrosc. **54**, 236A (2000).

[43] T. Morawietz, O. Marsalek, S. R. Pattenaude, L. M. Streacker, D. Ben-Amotz, and T. E. Markland, J. Phys. Chem. Lett. **9**, 851 (2018).

[44] A. D. Bond, K. A. Solanko, S. Parsons, S. Redder, and R. Boese, CrystEngComm **13**, 399 (2011).

[45] E. L. Crowell, Z. A. Dreger, and Y. M. Gupta, J. Mol. Struct. **1082**, 29 (2015).

[46] J.-P. Brog, C.-L. Chanez, A. Crochet, and K. M. Fromm, RSC Adv. **3**, 16905 (2013).

[47] P. Vishweshwar, J. A. McMahon, M. Oliveira, M. L. Peterson, and M. J. Zaworotko, J. Am. Chem. Soc. **127**, 16802 (2005).

[48] M. Takahashi, Crystals **4**, 74 (2014).

[49] J. Nyman and G. M. Day, Phys. Chem. Chem. Phys. **18**, 31132 (2016).

[50] K. Adhikari, K. M. Flurchick, and L. Valenzano, Chem. Phys. Lett. **621**, 109 (2015).

[51] M. A. Neumann and M. A. Perrin, CrystEngComm **11**, 2475 (2009).

[52] C. Qu and J. M. Bowman, Phys. Chem. Chem. Phys. **21**, 3397 (2019).

[53] G. Mathias and M. D. Baer, J. Chem. Theory Comput. **7**, 2028 (2011).

[54] G. Mathias, S. D. Ivanov, A. Witt, M. D. Baer, and D. Marx, J. Chem. Theory Comput. **8**, 224 (2012).

[55] Small differences in the spectra of paracetamol forms I and II (high-frequency region) with respect to what was published by us in Ref. [20] stem from the fact that the lattice constants reported in Ref. [51] were used in that reference, whereas here we use the experimental ones reported in Table I.

[56] M. Boczar, M. J. Wójcik, K. Szczeponek, D. Jamróz, A. Ziba, and B. Kawałek, Chem. Phys. **286**, 63 (2003).

[57] S. Roy, B. Chamberlin, and A. J. Matzger, Org. Process Res. Dev. **17**, 976 (2013).

[58] N. Raimbault, A. Grisafi, M. Ceriotti, and M. Rossi (unpublished).

[59] N. Raimbault, V. Athavale, and M. Rossi, http://dx.doi.org/10.17172/NOMAD/2019.01.25-1 (2019).